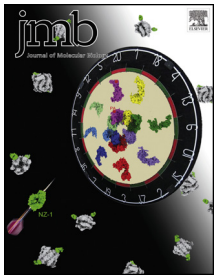

Structural Basis for the Selective Inhibition of c-Jun N-Terminal Kinase 1 Determined by Rigid DARPin–DARPin Fusions

Yufan Wu, Annemarie Honegger, Alexander Batyuk, Peer R.E. Mittl and Andreas Plückthun

Department of Biochemistry, *University of Zürich, Winterthurerstrasse 190, CH-8057 Zürich, Switzerland*

Correspondence to Andreas Plückthun: *plueckthun@bioc.uzh.ch*
https://doi.org/10.1016/j.jmb.2017.10.032
Edited by Amy Keating

Abstract

To untangle the complex signaling of the c-Jun N-terminal kinase (JNK) isoforms, we need tools that can selectively detect and inhibit individual isoforms. Because of the high similarity between JNK1, JNK2 and JNK3, it is very difficult to generate small-molecule inhibitors with this discriminatory power. Thus, we have recently selected protein binders from the designed ankyrin repeat protein (DARPin) library which were indeed isoform-specific inhibitors of JNK1 with low nanomolar potency. Here we provide the structural basis for their isotype discrimination and their inhibitory action. All our previous attempts to generate crystal structures of complexes had failed. We have now made use of a technology we recently developed which consists of rigid fusion of an additional special DARPin, which acts as a crystallization enhancer. This can be rigidly fused with different geometries, thereby generating a range of alternative crystal packings. The structures reveal the molecular basis for isoform specificity of the DARPins and their ability to prevent JNK activation and may thus form the basis of further investigation of the JNK family as well as novel approaches to drug design.

Introduction

Given their roles in signal transduction and pathology, the mitogen-activated protein kinases (MAPKs) have been extensively studied to understand the molecular mechanisms of kinase regulation. The extracellular signal-regulated protein kinases (ERKs), the c-Jun N-terminal kinases (JNKs) and the p38 family are three major subfamilies of the MAPK family [1–8].

The ERK1/2 pathway is predominantly responding to growth factors (e.g., EGF, FGF, PDGF), and ERK1/2 phosphorylate a number of substrates important for cell proliferation, cell cycle progression, cell division and differentiation. In contrast, MAPKs from the JNK and p38 families are mainly responsive to stress stimuli, such as pro-inflammatory cytokines, ionizing irradiation, heat shock, and osmotic shock, and they control pathways such as cell differentiation, apoptosis and autophagy [9–12].

JNKs were originally identified as kinases that phosphorylate c-Jun within its transcriptional activation domain, but today, almost 100 targets have been implicated, including transcription factors (Jun, ATF2, Myc, Elk1, NFAT4), cytoplasmic proteins involved in cytoskeleton regulation (DCX, Tau, WDR62) or vesicular transport (JIP1, JIP3), membrane receptors (BMPR2), and mitochondrial proteins (Mcl1, Bim). Similarly, p38s also have some unique targets (e.g., the MAP kinase-activated protein kinases 2 and 3), such that both JNKs and p38s are needed in response to various stress stimuli.

Three steps trigger the phosphorylation of MAPK substrates. During the first step, MAPK kinase kinases (MAP3Ks) are activated by extrinsic or intrinsic stimuli. Subsequently, MAP3Ks phosphorylate and activate MAPK kinases (MAP2K), which finally leads to two phosphorylation events within the activation loop of MAPKs.

The MAPK pathways are very diverse, involving many different MAP3Ks from the Ser/Thr protein kinase family (e.g., MEKKs, MLK3 and ASKs). While the ERK1/2 pathway is largely separated from the others, mammalian p38 and JNK kinases have most of their activators shared at the MAP3K level (e.g., MEKK1, MEKK4, ASK1, TAK1, MLK3, TAOK1). In contrast to

that, the second step is rather specific. Two highly specific STE family kinases, MKK4 and MKK7, are the two most important MAP2Ks in the JNK signaling cascade, although a few other MAP2Ks activate both JNK (MKK7) or p38 (MKK3 and MKK6) (reviewed in refs. [13,14]).

Another layer of complexity is added by scaffold proteins, such as the scaffold protein JNK-interacting protein 1 (JIP1), and by feedback phosphorylation of MAP3Ks by JNKs. Inactivation of JNKs is achieved by Ser/Thr and Tyr protein phosphatases, such as MAPK phosphatase 7 (MKP7) (reviewed in refs. [13,14]).

The JNK family is very diverse. In mammals, 10 highly similar isoforms are expressed by alternative splicing events of three different genes (*jnk1*, *jnk2* and *jnk3*; also called *mapk8*, *mapk9* and *mapk10*) and five more isoforms have been suggested by UniProt. Both JNK1 and JNK2 are ubiquitously expressed, while JNK3 expression is restricted to the brain, heart and testis [15]. Alternative splicing at two different sites generates four different JNK isoforms. Differential splicing within protein kinase subdomains IX and X generates α and β variants of JNK1 and JNK2. Isoforms with molecular masses of 46 and 54 kDa (distinguished by appending *1* and *2* to the kinase name, respectively) are generated by alternative splicing at the C-terminus [16].

Since JNKs regulate apoptosis, several lines of evidence implicate that JNKs are involved in tumor suppression [17,18]. Knockdown of JNK1 and JNK2 by small interfering RNA impaired apoptosis in response to anticancer drugs [19]. JNK1-deficient mice are highly susceptible to tumor development [20,21] and many tumor cell lines show impaired JNK signaling [22,23]. Furthermore, JNKs can sensitize cancer cells to genotoxic stress-induced cell death [24–26].

Consequently, we are currently challenged with finding new isoform-selective inhibitors to further investigate and combat JNK-dependent pathologies. Several JNK-directed inhibitors targeting the ATP-binding site have been developed [4,27]. Unfortunately, the ATP-binding site is highly conserved among JNK isoforms and protein kinases in general, which makes it extremely difficult to achieve selectivity among JNK isoforms. Hence, many nucleotide mimetics elicit unfavorable side effects, due to the lack of isoform specificity (reviewed in ref. [28]). Alternative sites for inhibition with greater diversity among JNK isoforms have been investigated, particularly peptide inhibitors that are often derived from known JNK interaction partners.

The docking groove for JIP1 is located close to the hinge region between the N- and C-terminal lobes, suggesting that the binding of motifs similar to JIP1 will exert allosteric changes in JNK kinases. Many JNK interaction partners, including upstream MAP2Ks, MAPK phosphatases, regulatory proteins and downstream substrates recognize JNK via this docking groove [29]. Since the docking grooves of JNK1, JNK2 and JNK3 are very similar and located far away from the activation loop, recruitment via this site is expected to be isoform- and activation state-independent. Many substrates can also be recognized by the FxF site, which is located in spatial proximity to the activation loop. This site was named based on the Phe-x-Phe-Pro sequence of linear ERK2 interaction partners [30]. The FxF site is also functional in JNKs [31].

Peptides derived from JIP1 or peptides that inhibit the interaction between JNK1 and c-Jun are promising candidates for isoform-specific inhibition [32,33]. To achieve even greater diversity, artificial JNK-binding proteins have been selected from combinatorial protein libraries. Traditionally, Fab fragments derived from monoclonal antibodies have been used for this purpose, but they would not be usable in the reducing cytoplasm, as they do not fold in the absence of disulfide bonds. More recently, several alternative frameworks have been investigated [34,35]. Designed ankyrin repeat proteins (DARPins) represent one class of such newer binding proteins. They are a family of small, highly stable binding proteins based on a repeat protein scaffold [36–38], which have been developed for biochemical research, diagnostics and therapy (reviewed in ref. [39]). They can be produced with high yields in *Escherichia coli*. Tightly packed repeats form a continuous hydrophobic core that is shielded from the solvent by specialized N- and C-terminal capping repeats (N-cap and C-cap). In DARPin libraries, six positions of each 33-amino-acid internal repeat are randomized. In selected binders, their surface forms a continuous paratope, stretching over the internal repeats, whose number typically varies between 2 and 3. Various selection methods such as ribosome display [37], phage display [40] and yeast surface display [41] have been used to select high-affinity binders from DARPin libraries.

To target novel binding epitopes JNK-directed binding proteins have been selected by ribosome display from a highly diverse combinatorial library of DARPins [42]. Selected binders were either isoform-specific or recognized both JNK1 and JNK2. In this study, we investigated DARPins J1_2_32, J1_4_7 and J1_8_27 that selectively bound isoform JNK1α1 but showed no affinity for JNK2α1 *in vitro*. Furthermore, these DARPins showed affinities in the low nanomolar range and isoform-specific inhibition of JNK activation *in vitro* [42]. To determine their epitopes on JNK1α1 and to elucidate the mechanism for isoform specificity, we were aiming to determine the crystal structures of JNK:DARPin complexes, but unfortunately, these complexes were not directly amenable to crystallization.

To overcome these issues, we applied the crystallization chaperone technique with DARPin D12 [43] as a crystallization enhancer (Fig. 1a) rigidly fused to the JNK-specific DARPins. Recently, it was shown that

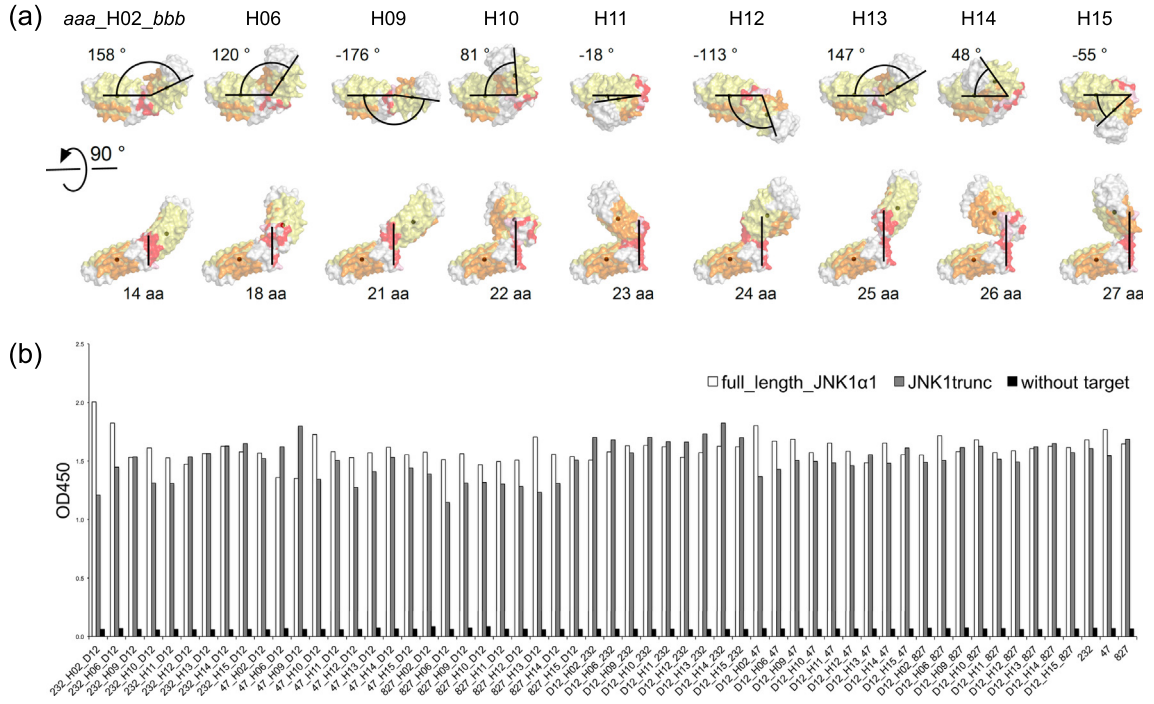

Fig. 1. (a) The DD rigid fusion concept. DD constructs are named aaa_Hxx_bbb, where aaa and bbb are the abbreviated names of the N- and C-terminal DARPin domains and Hxx indicates the length of the shared helix (with xx ranging from 02 to 15). The pseudo-torsion angle of the relative domain orientation and the amino acid number of the shared helix are shown for each DD construct. The DD constructs are shown with the N-terminus of the first DARPin to the left and the axis of the shared helix perpendicular to the image plane (top row) or vertically in the image plane (bottom row). (b) The JNK1α1-specific DARPins (DARPin 232, 47, 827) were inserted either into the N-terminal or the C-terminal position of all 9 DD frameworks, with crystallization-enhancing DARPin D12 providing the other paratope, yielding 54 different DD constructs. All 54 fusions were tested for binding to full-length JNK1α1 and $JNK1_{trunc}$. White bars, full-length JNK1α1; gray bars, $JNK1_{trunc}$; black bars, without target.

rigid fusions between either the N- or C-terminal capping repeats of the target-directed DARPin and a crystallization enhancer, such as D12, can promote crystal formation by giving rise to a series of potential crystal contacts with tunable geometry, and thus act as crystallization chaperones [44]. Here, we describe the crystal structures of a truncated version of JNK1α1 in complex with DARPin–DARPin (DD) rigid fusions comprising JNK1-specific DARPin domains. The structures reveal the molecular basis for isoform specificity of DARPins J1_2_32 and J1_4_7, and their ability to prevent JNK activation *in vitro*.

Results

DD constructs bind JNK1α1

Previously, ribosome display had been used to select three different DARPins that bind and inhibit human c-Jun N-terminal kinase JNK1α1 (MAPK8, UniProtKB P45983-2), but show little to no cross-reactivity with JNK2α1 (MAPK9, UniProtKB P45984-2) [42]. All attempts to crystallize the selected DARPins in complex with JNK1α1, in order to elucidate the mechanism of this discrimination, had previously failed. In order to obtain crystals of selected DARPins with JNK1α1, we applied the DD rigid fusion strategy [44,45]. DD constructs are named aaa_Hxx_bbb (Fig. 1a), where aaa and bbb are the abbreviated names of the N- and C-terminal DARPin domains and Hxx indicates the length of the shared helix (with xx ranging from 02 to 15). The ligand, for example, JNK1α1, is inserted right after the name of the cognate DARPin domain. A colon separates the DARPin domain from its ligand. The JNK1α1-specific DARPins were inserted into either the N-terminal or the C-terminal position of the DD framework, with DARPin D12 as the crystallization enhancer. DARPins J1_2_32, J1_4_7 and J1_8_27 [42] are abbreviated as 232, 47 and 827, respectively.

Three different DARPins at two positions and nine connector geometries resulted in 54 constructs that were all expressed in *E. coli*. All 54 DD proteins were characterized and their abilities to bind both full-length or truncated JNK1α1 were tested by ELISA (Fig. 1b). All ELISA signals of DD constructs were similar to each other and to the signals of the isolated DARPins, suggesting that the fusion did not impair their abilities to bind the target, and that all geometries were

suitable for target binding. For these ELISAs, we used both full-length JNK1α1 and a version (termed $JNK1_{trunc}$), in which 21 residues from the C-terminus of JNK1α1 were removed (equivalent to residues 364–384).

Crystal structure of $JNK1_{trunc}$ in complex with D12_H10_47

After initial characterization of all 54 DD proteins, 12 constructs based on frameworks with connectors H10 and H11 were selected for crystallization trials. A peptide fragment of the scaffolding protein JIP1 (c-Jun-amino-terminal kinase-interacting protein 1) was added to stabilize $JNK1_{trunc}$ for crystallization [46], and for simplicity, we still refer to the peptide as JIP1. All 12 DD constructs were monomeric at a concentration of 10 μM and bound $JNK1_{trunc}$, as indicated by a shift of the size exclusion chromatography (SEC) peak from the unliganded DD constructs to the complex with the expected molecular weight (Fig. S1). Four out of 12 DD:$JNK1_{trunc}$:JIP1 complexes yielded crystals, and the structures of two of them were determined. We neglected the remaining crystals, because they diffracted X-rays very poorly. The ternary complex D12_H10_47:$JNK1_{trunc}$:JIP1 crystallized in space group $P6_5$ and was refined at 2.7-Å resolution with one complex per asymmetric unit (Table 1). At a contour level of 1σ, the map shows clear density for residues 7 to 362 from $JNK1_{trunc}$ (except residues 33 to 38 and 182 to 185), residues 11 to 325 from D12_H10_47, and residues 154 to 163 from JIP1 (Fig. 2a).

The structure clearly depicts the 47 epitope on $JNK1_{trunc}$. Residues 253 to 265 of $JNK1_{trunc}$ form an α-helix, which is recognized by internal repeats 1 and 2 from 47 (Fig. 2b). This helix is part of the MAPK-specific insert region and thus unique to the MAPKs and a few related protein kinases [3]. Upon binding, a surface area of 1129 $Å^2$ is buried in the interface. Particularly Thr255 and Thr258 from $JNK1_{trunc}$ are pointing into amphipathic pockets involving Leu204, Met212, Leu242 and Leu275 on D12_H10_47. The interface also involves H-bonds between the Thr258 side chain from $JNK1_{trunc}$ and side chains from Asp233 and Thr237 from D12_H10_47. A secondary contact exists between the C-cap of 47 and both lobes of $JNK1_{trunc}$. Here Arg69 from $JNK1_{trunc}$ forms a salt bridge with Glu315 from D12_H10_47 and the side chain of Arg150 from $JNK1_{trunc}$ forms H-bonds with the main chain of Ile310 and Asp311 from the C-cap.

Table 1. Data collection and refinement statistics.

	D12_H10_47:$JNK1_{trunc}$:JIP1	232:$JNK1_{trunc}$:JIP1_H11_D12
Data collection		
Resolution range (Å)	46.959–2.700 (2.770–2.700)	49.383–3.200 (3.314–3.200)
Space group	$P6_5$	$C121$
Polypeptide chains/AU	3 (1 complex)	9 (3 complexes)
Unit cell parameters		
a, *b*, *c* (Å)	76.995, 76.995, 330.725	219.99, 141.76, 119.85
α, *β*, *γ* (°)	90, 90, 120	90, 97.828, 90
Observed reflections	1,246,432 (95,393)	413,476 (42,096)
Unique reflections	30,294 (2261)	58,948 (5875)
Multiplicity	41.1 (42.2)	7.0 (7.2)
Completeness (%)	99.9 (100)	97.94 (98.46)
Mean *I*/sigma(*I*)	22.99 (1.10)	11.27 (1.13)
CC(1/2)	1 (0.635)	0.998 (0.420)
Wilson *B*-factor	98.05	107.68
Refinement		
Resolution range (Å)	46.959–2.700 (2.770–2.700)	49.383–3.200 (3.314–3.200)
R_{work} (%)	20.18	18.60
R_{free} (%)	22.59	22.10
Protein atoms	5283	16,073
rmsd of bond lengths	0.002	0.003
rmsd of bond angles	0.458	0.567
Average *B*-factor ($Å^2$)	129.7	114.5
Ramachandran plot (%)		
Favored	95.76	97.63
Allowed	4.24	2.37
Outliers	0	0
Crystallization condition	PEG 10000 3% w/v Hepes 0.1 M, pH 6.8 Additives (0.033% w/v) 1,5-Naphthalene-disulfonic acid disodium salt 2,5-Pyridinedicarboxylic acid 3,5-Dinitrosalicylic acid	Lithium sulfate 1.8 M Tris 0.1 M, pH 8.5 Additives (0.002% w/v) Adenosine, Pepstatin A (±)-Epinephrine Sodium phenyl phosphate dibasic dehydrate Inosine 5-triphosphate trisodium salt

Values in parentheses refer to the outermost resolution shell.

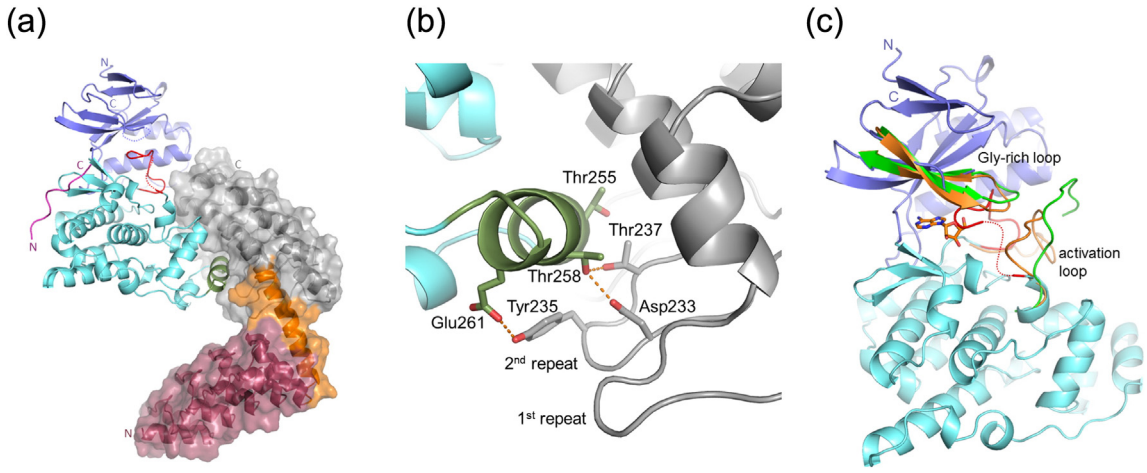

Fig. 2. Crystal structure of $JNK1_{trunc}$ in complex with D12_H10_47. (a) Overview of the D12_H10_47:$JNK1_{trunc}$:JIP1 complex. Residues without electron density are sketched as dotted lines. The color code of $JNK1_{trunc}$ refers to JIP1 (magenta), 47-recognition helix (dark green), activation and Gly-rich loops (red), small (dark blue) and large (light blue) kinase lobes. The DD is shown as a transparent surface with crystallization-enhancing DARPin D12 (dark red), shared helix H10 (orange) and cognate DARPin 47 (gray). (b) Close-up view of the $JNK1_{trunc}$:47 interface. Kinase residues 254–264 and 47 residues 199–238 are shown in dark green and gray, respectively. Broken lines in orange indicate H-bonds. (c) Superposition of $JNK1_{trunc}$ in complex with D12_H10_47 (coloring like in image a), in complex with 232_H11_D12 (orange carbon atoms including adenosine), and in complex with 4-phenyl-7-azaindole (PDB ID: 4AWI, green). Identical parts have been omitted.

The structure of $JNK1_{trunc}$ in complex with D12_H10_47 is similar to other JNK1α1:inhibitor complex structures (e.g., PDB ID: 4AWI [47], 0.77 Å rmsd for 303 Cα atoms). However, a major difference exists for the conformation of the activation loop (residues 173 to 181). In the D12_H10_47:$JNK1_{trunc}$:JIP1 complex, these residues fold back into the ATP-binding pocket, displacing the ligand, which is present in many JNK1:inhibitor complex structures (Fig. 2a, c). In many JNK1:inhibitor complex structures, residues 173 to 183 form a flexible loop between the small and large kinase lobes. In contrast to that, the inward facing conformation in the D12_H10_47:$JNK1_{trunc}$:JIP1 structure is stabilized by intra-molecular H-bonds between the side chains of Lys55, Glu73 and Thr175 and main chain atoms of residues 171, 175 and 176. Active site residues Lys55 and Glu73 guide the orientation of ATP by direct interactions between the side chain of Lys55 with the α- and β-phosphates (reviewed in ref. [48]). In the D12_H10_47:$JNK1_{trunc}$:JIP1 structure, residues 175 to 179 are shielding Lys55 and Glu73. Residues 175 to 179 are oriented by a β-hairpin at the beginning of this stretch, which is stabilized by an H-bond between Ala173-N and the Glu315 side chain from the D12_H10_47 C-cap (Fig. S2). Unfortunately, the side chains of Lys55 and Glu315 are poorly defined in the electron density map.

Crystal structure of $JNK1_{trunc}$ in complex with 232_H11_D12

In the 232_H11_D12 construct, the JNK1α1-specific DARPin is located at the N-terminus, whereas in D12_H10_47, it is located at the C-terminus. Furthermore, the orientation of the DARPins in the rigid fusion protein is different, because the linker length differs by one amino acid. The differences in construct design generate differences in crystal packing. The ternary complex 232:$JNK1_{trunc}$:JIP1_H11_D12 crystallized in space group *C*121 and was refined at 3.2 Å (Table 1). The electron density map shows continuous density at 1σ contour level for residues 8 to 362 from $JNK1_{trunc}$, residues 6 to 325 from 232_H11_D12 chain A, and residues 154 to 163 from JIP1 chain I. Difference electron density at the ATP-binding site was interpreted as an adenosine from the reservoir solution (Fig. 3a). The N-terminal His_6-tag of 232_H11_D12 is partially visible in the electron density map, because it is involved in a crystal contact. The asymmetric unit contains three 232:$JNK1_{trunc}$:JIP1_H11_D12 complexes that form a distorted trimer (Fig. 3b). Within the trimer, there is no direct interaction between $JNK1_{trunc}$ chains, and the trimer is generated between DARPin:kinase contacts only. Therefore, the H11 helix is crucial for the stability of the crystallographic trimer. Crystal lattice forces in combination with some plasticity of the H11 helix exert the distortion of the trimer.

Each 232_H11_D12 construct makes contact to two $JNK1_{trunc}$ chains, via the cognate DARPin 232, and the crystallization enhancer D12. The 232 epitope on $JNK1_{trunc}$ is almost identical to the 47 epitope, comprising residues 253 to 262 from $JNK1_{trunc}$ and residues 22 to 110 from 232_H11_D12. Just as in the D12_H10_47:$JNK1_{trunc}$:JIP1 structure, Thr255 and Thr258 point into amphipathic pockets on cognate DARPin 232. Residues 175 to 178 from $JNK1_{trunc}$ form

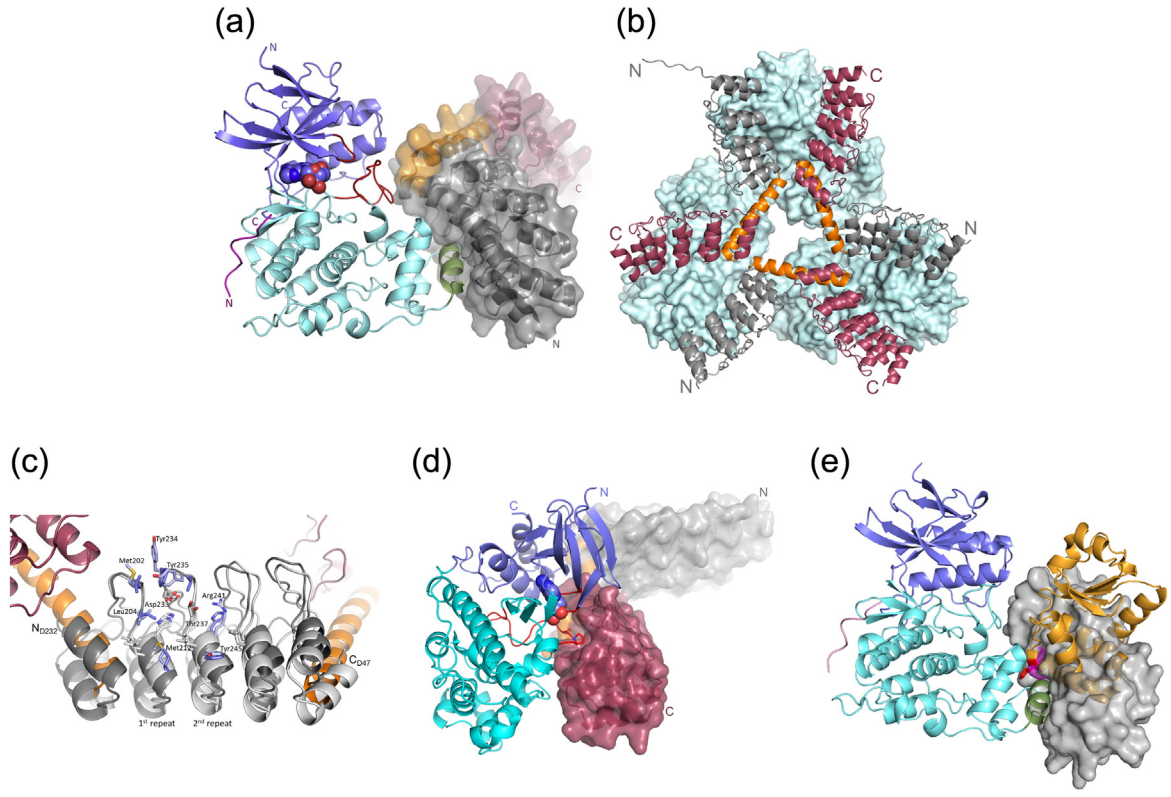

Fig. 3. Crystal structure of $JNK1_{trunc}$ in complex with 232_H11_D12. (a) Overview of the 232:$JNK1_{trunc}$:JIP1_H11_D12 complex. Orientation and color code similar to Fig. 2a. Adenosine is shown as spheres. (b) The asymmetric unit contains a distorted trimer. The $JNK1_{trunc}$ kinases and the cognate 232 DARPins are shown as light blue surfaces and gray ribbons, respectively. The crystallization-enhancing D12 (red) forms a non-cognate interface and the shared helices H11 (orange) bridge the gaps in the trimer. (c) Superposition of 232_H11_D12 (dark gray, 232 domain) on D12_H10_47 (light gray, 47 domain) based on the superposition of $JNK1_{trunc}$ (not shown). D12 and shared helix are shown as in image a. Residues that are identical in 232 and 47 are shown with gray carbon atoms; similar residues are shown with light blue (47) and dark blue (232) carbon atoms. Residue numbering according to 47 (see Fig. 2b). (d) Non-cognate $JNK1_{trunc}$:D12 interface. Color coding same as above. The $JNK1_{trunc}$ kinases are rotated approximately 90° around the vertical axis compared to the view in image a. D12 makes contacts to the activation loop (side chains shown as sticks with red carbon atoms). (e) Superposition of the 232:$JNK1_{trunc}$:JIP1_H11_D12 complex on JNK1:MKP7 (PDB ID: 4YR8, [49]). Color coding of $JNK1_{trunc}$:JIP1 as above. 232_H11_D12 is shown as a gray surface (D12 not shown). The location of Phe88 is highlighted in magenta. MKP7 is shown as an orange cartoon with Phe285 depicted as red sticks.

a secondary interaction site with residues 154 to 157 from the C-terminal connector repeat of 232. Binding modes of 232 and 47 are identical because most residues of the paratopes are conserved (Fig. 3c). Residues Asp77, Thr81, Leu86, and Leu119 at the center of the interface in 232 are identical to residues Asp233, Thr237, Leu242, and Leu275 in 47, and residues Leu46, Ile56, Phe78, Val79, Phe89, Leu90, and Leu114 at the periphery of the interface in 232 are similar to residues Met201, Met212, Tyr234, Tyr235, Tyr245, Ile246, and Thr270 in 47, respectively. Upon binding, the 232:$JNK1_{trunc}$ interface buries an average surface area of 836 ± 123 $Å^2$ (calculated by PDBe-PISA, average of three complexes in the trimer).

Interestingly, the cognate 232:$JNK1_{trunc}$ interface (which depicts an interaction with low nanomolar K_D [42]) is smaller than the non-cognate D12:$JNK1_{trunc}$ interface, which has a buried surface area of 1322 ± 88 $Å^2$. DARPin D12, the crystallization enhancer, was originally selected to recognize the V3 loop of human immunodeficiency virus envelope glycoprotein gp120 [43]. D12 can form a non-cognate interface not only with itself but also with $JNK1_{trunc}$, where it recognizes the activation loop formed by residues 182 to 187. The side chains of Met182 and Pro184 from $JNK1_{trunc}$ are sandwiched between the side chains of His238/Tyr246 and Phe205/Trp213 from 232_H11_D12, respectively (Fig. 3d). In addition, the Tyr185 side chain from $JNK1_{trunc}$ forms H-bonds with the side chains of Asp267 and Thr271 from 232_H11_D12. However, these interactions are not strong enough to be detectable in solution, as the isolated complex contains 232_H11_D12 with only one kinase molecule (Fig. S1).

The glycine-rich loop (residues 33 to 38), which is disordered in the D12_H10_47:JNK1$_{trunc}$:JIP1 structure, is well defined in the 232:JNK1$_{trunc}$:JIP1_H11_D12 complex structure and adopts a similar conformation as in PDB ID: 4AWI (Fig. 2c). Comparison with other JNK1α1:inhibitor complex structures reveals that the activation loop, which is formed by residues 173 to 181, adopts yet another conformation. This loop, which is partially disordered in all JNK1α1 structures determined before (e.g., residues 174 to 178 are disordered in PDB ID: 4AWI), is stabilized by the non-cognate D12 interaction and clearly visible in the electron density map of the 232:JNK1$_{trunc}$:JIP1_H11_D12 complex. Compared to 4AWI, residues 180 to 187 are moved approximately 6 to 8 Å toward the nucleotide binding pocket (Fig. 2c).

Superposition of the D12_H10_47:JNK1$_{trunc}$:JIP1 and 232:JNK1$_{trunc}$:JIP1_H11_D12 structures based on the JNK C-lobe (residues 150 to 360) reveals that the largest differences are seen for the loop formed by residues 281 to 289. In the 232:JNK1$_{trunc}$:JIP1_H11_D12 structure, Lys288-Cα has moved 9 Å toward the JIP1 peptide. Since this loop is not involved in crystal contacts in any of the two structures, there is no obvious reason for this movement. Perhaps these differences reflect the intrinsic flexibility of the loop region (Fig. S3).

This superposition also reveals that in the 232:JNK1$_{trunc}$:JIP1_H11_D12 structure, the N-lobe has moved approximately 3 Å (Asp17-Cα) toward the D12 domain, closing the active site pocket. This movement is a consequence of the rearrangement of the activation loop. In the D12_H10_47:JNK1$_{trunc}$:JIP1 structure, the activation loop binds deep in the active site pocket, whereas in the 232:JNK1$_{trunc}$:JIP1_H11_D12 structure, it has moved out of the active site and forms non-cognate interactions with D12. A gentle rotation between N- and C-lobes is frequently observed for JNKs and protein kinases in general (Fig. S3).

The conformations of the N-lobe seen in the 232:JNK1$_{trunc}$:JIP1_H11_D12 structure resembles the conformation of JNK1 in complex with the catalytic domain of MKP7 (PDB ID: 4YR8, [49]), a MAPK phosphatase and negative regulator of JNK. Although in the JNK1:MKP7 complex, the activation loop is disordered, MKP7 occupies a similar position like DARPins 47 and 232. MKP7 recognizes the FxF site of JNK1, which involves residues from the DARPin paratope (residues 255 and 256). Rearrangement of residues 281–289 is also observed in the JNK1:MKP7 complex structure. However, two distinct 232_H11_D12 molecules that are related by non-crystallographic symmetry either stabilize the activation loop via the D12 domain or bind to the FxF site via the target-binding domain. In the JNK1:MKP7 structure residues, Phe285–Asn286–Phe287 define the FxF motif of MKP7. Here, the side chain of Phe285 penetrates a cleft on JNK1 (Fig. 3e). Phe88 and Tyr245 mimic this side chain in molecules 232_H11_D12 and D12_H10_47, respectively, although Phe285 from MKP7 penetrates JNK1 much deeper than any of the DARPin residues.

Discussion

Previously, ribosome display had been used to select for binders to the short splice variants of JNK1 and JNK2, and three different binders had been identified with low nanomolar affinities to JNK1α1 that discriminate between JNK1 and JNK2, despite binding to the highly conserved kinase core [42]. While complexes of the selected DARPins with JNK1α1 did not yield any crystals, two different DD fusion constructs allowed us to determine the structures of 232 and 47 in complex with the kinase, while 827 still failed to yield crystals. 232 and 47 were found to recognize essentially the same epitope on JNK1$_{trunc}$, which is in the MAPK-specific insert region of the kinase, although all but three randomized positions as well as two non-randomized framework positions differ between 47 and 232.

The discrimination between JNK1 and JNK2, enforced by the selection strategy [42], can directly be explained by the structures (Figs. 2a, 3a): three of the sequence differences between JNK1 and JNK2 fall within the epitope recognized by 232: Gly177 → Cys, Tyr230 → His and Thr258 → Asn, the latter two are also within the epitope of 47 (Fig. 2b). The 47 paratope extends to the C-cap of D12_H10_47, or in the case of 232_H11_D12 to the connector module, although the involvement of these residues varies between the three copies in the asymmetric unit. Thr258 is at the heart of the interface and its side chain explores the amphipathic character of the DARPin:kinase interaction by H-bonds and hydrophobic contacts (Fig. 2b). Since asparagine would be unable to satisfy these constraints, it is expected that particularly the Thr258 → Asn mutation diminishes the affinities of DARPins 232 and 47 for JNK2.

While complex 232:JNK1$_{trunc}$:JIP1_H11_D12 was monomeric in solution (Fig. S1), in the asymmetric unit of the crystal, it forms a trimer (Fig. 3a). The cognate and non-cognate contacts of 232 and D12, respectively, together mediate the trimerization of the complex. Interestingly, the non-cognate contact buries a larger surface area than the isoform-specific 232:JNK1$_{trunc}$ interaction. Since the D12:JNK1$_{trunc}$ interaction is not observed in the D12_H10_47:JNK1$_{trunc}$:JIP1 structure, it is probably very weak, and gel filtration indicates that it does not form in solution. Thus, the buried surface area alone is not indicative for the biological significance or strength of this interaction. This lack of relationship has been reviewed previously [50]: although there is a correlation between binding affinity and the amount of surface area buried at the interface, for a given amount

of surface area buried, the binding affinity (K_D) spans 4 orders of magnitude, and no obvious relationship between binding affinity and the chemical composition of the interface can be found.

The DARPin D12 was originally selected against a cyclized HIV gp120 V3 loop mimetic with the sequence KRIHIGPGRAFYTT^{D}PP, and this loop has a completely different conformation than the JNK loop occupying a similar space near DARPin D12 (manuscript under preparation). Nonetheless, one residue Tyr185 from the activation loop of $JNK1_{trunc}$ takes a remarkably similar space to Tyr12 from the V3 loop peptide, and engages in the same interactions with and Asp and Thr side chain on the DARPin loop. Other weak interactions contribute to these crystal contacts between JNK and DARPin D12.

Binding of 232 and 47 to $JNK1_{trunc}$ causes conformational changes in the glycine-rich- and activation loops that are lining the ATP-binding site of JNK1. Binding of 47 exerts the formation of a β-turn conformation of residues 171 to 174 that pushes the activation loop into the ATP-binding pocket where it interacts with active site residues from the small lobe. To assume this loop conformation, Gly171 and Gly177 adopt main-chain dihedral angles that are disallowed for non-glycine residues. In some cancer cell lines, Gly171 and Gly177 are mutated to serine and arginine, respectively [51]. These mutations could prevent the observed conformation of residues 171 to 180 rendering JNK1 constitutively active. Furthermore, Thr183 and Tyr185 are no longer accessible for phosphorylation by MAPK kinases. The protecting activity of 232 is less obvious, because in the 232:$JNK1_{trunc}$:JIP1_H11_D12 structure, the crystallization enhancer D12 interacts unspecifically with Tyr185. However, the side chain of Tyr185 points toward the solvent. In this conformation, Tyr185 could be phosphorylated by upstream kinases, provided that the conformation of this loop is sufficiently stable in the absence of D12.

Binding of D12_H10_47 and 232_H11_D12 causes gentle rotations of the N-lobe relative to the C-lobe, which is within the range generally seen among different JNK crystal structures. Whether this rotation is induced by DARPins 232 and 47 alone or whether the D12 fusion contributes to this rotation is currently unknown. The movement of the N-lobe is influenced by the conformations of the active site loops, and at least in the 232:$JNK1_{trunc}$:JIP1_H11_D12 structure, these conformations are influenced by the D12 domain.

The 232:$JNK1_{trunc}$:JIP1_H11_D12 structure reveals that D12 protects Tyr185 from phosphorylation, but unfused 232 also protects JNK1α1 from phosphorylation in the absence of D12 [42]. It is possible that the bulk of the bound cognate DARPin sterically protects JNK1 from approach of the activating upstream kinase, which is supported by the observation that DARPin 232 occupies the FxF site, which is probably necessary for the recruitment of MAP2K.

In summary, we determined the binding modes of DARPins 232 and 47 and deciphered the molecular reasons for their JNK1α1 specificity. DARPins 232 and 47 recognize JNK1 via the FxF site, and could be thus useful in masking this site in functional assays, also in the development of new inhibitors. This analysis became only possible by fusing the DARPins with the crystallization-enhancing D12 molecule. The application of this method was reported previously [45], where it was shown that D12 forms dominant crystal contacts between D12 paratopes. The current analysis extends this interpretation, as in the D12_H10_47:$JNK1_{trunc}$:JIP1 structure, and in the 232:$JNK1_{trunc}$:JIP1_H11_D12 structure, D12 is involved in crystal contacts, albeit with other parts of the molecules. Thus, the D12-fusion strategy was highly effective for crystallizing these DARPin:kinase complexes.

Materials and Methods

Expression and purification of DD fusion proteins

DD fusion proteins were expressed from the plasmid pQE30ss (vector pQE30 with double stop codon) in the *E. coli* strain XL1-blue. The fusion proteins contain an N-terminal MRGS-His_6 tag. An overnight culture of each variant was prepared as follows: 50 mL 2xYT medium (100 mg/L ampicillin, 1% w/v glucose) was inoculated with a single colony cultured on LB plates (100 mg/L ampicillin, 1% w/v glucose, 1.5% agar). The overnight culture (225 rpm, 37 °C) typically reached an OD_{600} of ~4.5. The seed cultures were then diluted to a final OD_{600} = 0.1 into 1 L of 2xYT medium (containing 100 mg/L ampicillin, 1% w/v glucose) in a 5-L baffled flask. Expression cultures were placed in a shaker (25 mm radius, 108 rpm, 30 °C) until induction with IPTG (0.5 mM final concentration) at OD_{600} ~ 0.6. Induced cultures were then allowed to shake for 18 h at 30 °C. Overnight expression cultures were harvested by centrifugation (5000*g*, 4 °C, 15 min).

Cell pellets from 1-L cultures were resuspended in 30 mL TBS_{400} buffer [50 mM Tris–HCl (pH 7.4), 400 mM NaCl] containing one EDTA-free protease inhibitor tablet (Roche), DNAse (10 μg), and $MgCl_2$ (10 mM final concentration), then homogenized with a Digitana YellowLine mixer and ruptured by one passage through a TS 1.1 Constant Cell Disrupter System at 30,000 psi. A subsequent sonication step (duty cycle 50%, intensity 5, 1–2 × 30 s pulses) was applied to the crude lysate for additional cell rupture and shearing of DNA. The lysate was clarified by centrifugation in SS34 tubes (30 min at 28,000*g*, 4 °C) to give a final volume of ~30 mL. The supernatant was then filtered (0.22 μm Millex GP, Millipore) with a sterile

syringe before adjusting the pH to ~8.0 with 0.5 M NaOH.

Immobilized metal-ion affinity chromatography on Ni^{2+}-nitrilotriacetic acid resin was used for protein purification at room temperature. Four milliliters of 50% slurry of Ni^{2+}-nitrilotriacetic acid Superflow (Qiagen) was applied to a 15-mL fitted chromatography column (Bio-Rad). Before application of the clarified supernatant, the column was washed with 5 column volumes (CV) of UHP water, and then equilibrated with 10 CV of TBS-W buffer [50 mM Tris–HCl (pH 7.4), 400 mM NaCl, 20 mM imidazole, 10% glycerol]. After applying the clarified lysate, a washing step with TBS-W (10 CV) was performed. Protein samples were eluted with 3 CV of TBS-E [50 mM Tris–HCl (pH 7.4), 400 mM NaCl, 250 mM imidazole, 10% glycerol]. The protein was aliquoted to 1 mL aliquots in Eppendorf tubes, frozen in liquid nitrogen and stored at −80 °C.

Expression and purification of kinase

The expression of $JNK1_{trunc}$ (res. 2–363 from UniProtKB entry P45983-2 with N-terminal MRGS-His_6 tag) was carried out in the same way as for DARPin-based fusion proteins described above, except that the temperature was changed to 18 °C after induction with IPTG (0.2 mM final concentration). Cell pellets from 1-L cultures were re-suspended in 80 mL Resuspension Buffer [10 mM Hepes (pH 7.0), 400 mM NaCl, 2 mM DTT, 10% (v/v) glycerol] containing one EDTA-free protease inhibitor tablet (Roche), DNAse (10 μg) and $MgCl_2$ (10 mM final concentration). The cell disruption step was carried out in the same way as described for DARPin-based fusion proteins above. After applying the clarified lysate on immobilized metal-ion affinity chromatography, washing steps were performed first by 20 CV of Wash Buffer [10 mM Hepes (pH 7.0), 400 mM NaCl, 2 mM DTT, 10% (v/v) glycerol, 20 mM imidazole] and followed by 20 CV of ATP Wash Buffer [10 mM Hepes (pH 7.0), 400 mM NaCl, 2 mM DTT, 10% (v/v) glycerol, 20 mM imidazole, 10 mM ATP, 10 mM $MgCl_2$]. The $JNK1_{trunc}$ sample was eluted with 3 CV of Elution Buffer [10 mM Hepes (pH 7.0), 400 mM NaCl, 2 mM DTT, 10% (v/v) glycerol, 250 mM imidazole]. Before freezing in liquid nitrogen, the buffer was exchanged to Freezing Buffer [10 mM Hepes (pH 7.0), 200 mM NaCl, 2 mM DTT, 10% (v/v) glycerol] on PD-10 desalting columns (GE Healthcare) according to the manufacturer's instructions. All steps were performed at 4 °C due to the instability of the kinase.

Purification of DD:$JNK1_{trunc}$ complexes

SEC was performed for the further purification of the complexes of DD fusion constructs with $JNK1_{trunc}$. A peptide fragment of the scaffolding protein JIP1 with the sequence RPKRPTTLNLF [res. 157–167 of human JIP1, res. 153–163 of murine JIP1, synthesized by LifeTein LLC (Hillsborough, NJ)] was used to stabilize $JNK1_{trunc}$ during purification and crystallization. Before applying to SEC, purified $JNK1_{trunc}$, DD and JIP1 were mixed at the molar ratio of 1:1:5 in SEC Buffer [10 mM Hepes (pH 7.0), 200 mM NaCl, 2 mM DTT, 5% (v/v) glycerol] and incubated on ice for 1 h to allow complex formation.

For every protein mixture, the peak fraction with the smallest molecular weight containing both DD fusion and $JNK1_{trunc}$ in equimolar amounts, as determined by SDS-PAGE, was collected and used for crystallization. All steps were performed at 4 °C.

ELISA

DD constructs were tested by ELISA to qualitatively assess binding to full-length JNK1α1 and $JNK1_{trunc}$. In this setup, 100 μL of 1 μM biotinylated JNK1α1 or $JNK1_{trunc}$ was immobilized on a Maxisorp plate pre-coated with Neutravidin and the plate was incubated with 100 μL of 200 nM DD constructs, carrying an N-terminal RGSHis_6 tag. Binding was detected with anti-RGS-His-antibody-HRP conjugate (QIAGEN) by measuring the absorbance at OD_{450}.

Crystallization

Eight commercially available grid screens of the in-house Protein Crystallization Center† were used for initial crystallization. The protein was concentrated to 10–25 mg/mL using an Amicon Ultra Centrifugal Filter Device (Millipore, USA) with a molecular weight cutoff of 10,000 Da. CrystalQuick crystallization plates (Greiner Bio-One) were used for the sitting drop method. The protein was mixed with the mother liquor in a volume ratio of 1:1, 1:2 and 2:1 for each single condition. Crystal growth took place at 4 °C.

Manual crystallization setups were performed with sitting-drop crystallization plates from Hampton Research. Reservoir solution (500 μL) was applied and the drop was mixed with the mother liquor in a volume ratio of 1:1, 1:2 and 2:1 for each single condition. The Silver Bullet and Silver Bullet Bio kits from Hampton Research were used for additive screening.

Data collection and processing

Data were collected from single, cryo-cooled crystals at beamlines PXI (Swiss Light Source, Villigen, Switzerland) with PILATUS 6M, high-resolution diffractometers. Data were processed and scaled with XDS [52].

To find the precise position of the domains, molecular replacement was performed with the following models as separate search models, JNK1β1 (PDB ID: 1UKI) and DARPin off7 (extracted from PDB ID: 1SVX), and designed models of DD constructs, omitting the shared

helix itself in the search model. The helix was subsequently built into the density visible between the two DARPin units.

Accession numbers

The atomic coordinates of structures D12_H10_47:JNK1$_{trunc}$:JIP1 and 232:JNK1$_{trunc}$:JIP1_H11_D12 have been deposited in the PDB as entries 6F5E and 5LW1, respectively.

Acknowledgments

We thank Beat Blattmann and Céline Stutz-Ducommun for their help in protein crystallization and the staff of beamline PXI at the Swiss Light Source, PSI, for support during data collection. We are grateful to Dr. Jing Dong, Jian Zhu and the members of the Plückthun laboratory for valuable discussions. Yufan Wu was supported by a predoctoral fellowship of the Forschungskredit from the University of Zürich. This work was supported by a Schweizerischer Nationalfonds grant (310030B_166676 to A.P.).

Appendix A. Supplementary data

Supplementary data to this article can be found online at https://doi.org/10.1016/j.jmb.2017.10.032.

Received 10 June 2017;
Received in revised form 30 October 2017;
Accepted 31 October 2017
Available online 8 November 2017

Keywords:
Kinases;
Designed Ankyrin Repeat Protein;
Protein engineering;
X-ray crystallography;
Crystallization Chaperone

Present address: Y. Wu, Paul Scherrer Institute, OFLC/106, 5232, Villigen PSI, Switzerland

Present address: A. Batyuk, Linac Coherent Light Source, SLAC National Accelerator Laboratory, 2575 Sand Hill Road, Menlo Park, CA 94025, USA

†www.bioc.uzh.ch/research/core-facilities/proteincrystallization-center/experimental-setup/initial-xtal-screens/

Abbreviations used:
DARPin, designed ankyrin repeat protein; DD, DARPin–DARPin rigid fusion construct; JNK1, full-length JNK1 splicing variant JNK1α1 (c-jun N-terminal kinase 1 alpha, mitogen-activated protein kinase 8, UniProtKB entry P45983-2); JNK1$_{trunc}$, C-terminally truncated JNK1α1 (res. 364–384 removed from full-length JNK1); JIP1, c-Jun-amino-terminal kinase-interacting protein 1, in this study the abbreviation refers to the peptide fragment that was used (aa seq: RPKRPTTLNLF); MAPKs, mitogen-activated protein kinases; ERKs, extracellular signal-regulated protein kinases; SEC, size exclusion chromatography.

References

[1] T.G. Boulton, S.H. Nye, D.J. Robbins, N.Y. Ip, E. Radziejewska, S.D. Morgenbesser, et al., ERKs: a family of protein-serine/threonine kinases that are activated and tyrosine phosphorylated in response to insulin and NGF, Cell 65 (1991) 663–675.
[2] M. Hibi, A. Lin, T. Smeal, A. Minden, M. Karin, Identification of an oncoprotein- and UV-responsive protein kinase that binds and potentiates the c-Jun activation domain, Genes Dev. 7 (1993) 2135–2148.
[3] A. Zeke, M. Misheva, A. Remenyi, M.A. Bogoyevitch, JNK signaling: regulation and functions based on complex protein–protein partnerships, Microbiol. Mol. Biol. Rev. 80 (2016) 793–835.
[4] A. Kumar, U.K. Singh, S.G. Kini, V. Garg, S. Agrawal, P.K. Tomar, et al., JNK pathway signaling: a novel and smarter therapeutic targets for various biological diseases, Future Med. Chem. 7 (2015) 2065–2086.
[5] E.T. Coffey, Nuclear and cytosolic JNK signalling in neurons, Nat. Rev. Neurosci. 15 (2014) 285–299.
[6] V. Sehgal, P.T. Ram, Network motifs in JNK signaling, Genes Cancer 4 (2013) 409–413.
[7] C. Tournier, The 2 faces of JNK signaling in cancer, Genes Cancer 4 (2013) 397–400.
[8] X. Sui, N. Kong, L. Ye, W. Han, J. Zhou, Q. Zhang, et al., p38 and JNK MAPK pathways control the balance of apoptosis and autophagy in response to chemotherapeutic agents, Cancer Lett. 344 (2014) 174–179.
[9] A.S. Dhillon, S. Hagan, O. Rath, W. Kolch, MAP kinase signalling pathways in cancer, Oncogene 26 (2007) 3279–3290.
[10] G. Huang, L.Z. Shi, H. Chi, Regulation of JNK and p38 MAPK in the immune system: signal integration, propagation and termination, Cytokine 48 (2009) 161–169.
[11] B.K. Kim, H.M. Kim, K.S. Chung, D.M. Kim, S.K. Park, A. Song, et al., Upregulation of RhoB via c-Jun N-terminal kinase signaling induces apoptosis of the human gastric carcinoma NUGC-3 cells treated with NSC12618, Carcinogenesis 32 (2011) 254–261.
[12] G.S. Hotamisligil, R.J. Davis, Cell signaling and stress responses, Cold Spring Harb. Perspect. Biol. 8 (2016) a006072.
[13] J.M. Kyriakis, J. Avruch, Mammalian mitogen-activated protein kinase signal transduction pathways activated by stress and inflammation, Physiol. Rev. 81 (2001) 807–869.
[14] Y.R. Chen, A. Shrivastava, T.H. Tan, Down-regulation of the c-Jun N-terminal kinase (JNK) phosphatase M3/6 and activation of JNK by hydrogen peroxide and pyrrolidine dithiocarbamate, Oncogene 20 (2001) 367–374.
[15] A.M. Bode, Z. Dong, The functional contrariety of JNK, Mol. Carcinog. 46 (2007) 591–598.

[16] S. Gupta, T. Barrett, A.J. Whitmarsh, J. Cavanagh, H.K. Sluss, B. Derijard, et al., Selective interaction of JNK protein kinase isoforms with transcription factors, EMBO J. 15 (1996) 2760–2770.
[17] R.J. Davis, Signal transduction by the JNK group of MAP kinases, Cell 103 (2000) 239–252.
[18] E.F. Wagner, A.R. Nebreda, Signal integration by JNK and p38 MAPK pathways in cancer development, Nat. Rev. Cancer 9 (2009) 537–549.
[19] N.V. Oleinik, N.I. Krupenko, S.A. Krupenko, Cooperation between JNK1 and JNK2 in activation of p53 apoptotic pathway, Oncogene 26 (2007) 7222–7230.
[20] Q.B. She, C. Huang, Y. Zhang, Z. Dong, Involvement of c-jun NH(2)-terminal kinases in resveratrol-induced activation of p53 and apoptosis, Mol. Carcinog. 33 (2002) 244–250.
[21] C. Tong, Z. Yin, Z. Song, A. Dockendorff, C. Huang, J. Mariadason, et al., C-Jun NH2-terminal kinase 1 plays a critical role in intestinal homeostasis and tumor suppression, Am. J. Pathol. 171 (2007) 297–303.
[22] C. Cellurale, N. Girnius, F. Jiang, J. Cavanagh-Kyros, S. Lu, D.S. Garlick, et al., Role of JNK in mammary gland development and breast cancer, Cancer Res. 72 (2012) 472–481.
[23] A. Hubner, D.J. Mulholland, C.L. Standen, M. Karasarides, J. Cavanagh-Kyros, T. Barrett, et al., JNK and PTEN cooperatively control the development of invasive adenocarcinoma of the prostate, Proc. Natl. Acad. Sci. U. S. A. 109 (2012) 12046–12,051.
[24] A. Sau, G. Filomeni, S. Pezzola, S. D'Aguanno, F.P. Tregno, A. Urbani, et al., Targeting GSTP1-1 induces JNK activation and leads to apoptosis in cisplatin-sensitive and -resistant human osteosarcoma cell lines, Mol. BioSyst. 8 (2012) 994–1006.
[25] I.S. Song, S.Y. Jun, H.J. Na, H.T. Kim, S.Y. Jung, G.H. Ha, et al., Inhibition of MKK7-JNK by the TOR signaling pathway regulator-like protein contributes to resistance of HCC cells to TRAIL-induced apoptosis, Gastroenterology 143 (2012) 1341–1351.
[26] F. Xiao, B. Liu, Q.X. Zhu, c-Jun N-terminal kinase is required for thermotherapy-induced apoptosis in human gastric cancer cells, World J. Gastroenterol. 18 (2012) 7348–7356.
[27] P. Koch, M. Gehringer, S.A. Laufer, Inhibitors of c-Jun N-terminal kinases: an update, J. Med. Chem. 58 (2015) 72–95.
[28] A. Messoussi, C. Feneyrolles, A. Bros, A. Deroide, B. Dayde-Cazals, G. Cheve, et al., Recent progress in the design, study, and development of c-Jun N-terminal kinase inhibitors as anticancer agents, Chem. Biol. 21 (2014) 1433–1443.
[29] J.D. Laughlin, J.C. Nwachukwu, M. Figuera-Losada, L. Cherry, K.W. Nettles, P.V. LoGrasso, Structural mechanisms of allostery and autoinhibition in JNK family kinases, Structure 20 (2012) 2174–2184.
[30] D.L. Sheridan, Y. Kong, S.A. Parker, K.N. Dalby, B.E. Turk, Substrate discrimination among mitogen-activated protein kinases through distinct docking sequence motifs, J. Biol. Chem. 283 (2008) 19511–19,520.
[31] N. Fernandes, D.E. Bailey, D.L. Vanvranken, N.L. Allbritton, Use of docking peptides to design modular substrates with high efficiency for mitogen-activated protein kinase extracellular signal-regulated kinase, ACS Chem. Biol. 2 (2007) 665–673.
[32] M.A. Bogoyevitch, Therapeutic promise of JNK ATP-noncompetitive inhibitors, Trends Mol. Med. 11 (2005) 232–239.
[33] K.R. Ngoei, B. Catimel, N. Church, D.S. Lio, C. Dogovski, M.A. Perugini, et al., Characterization of a novel JNK (c-Jun N-terminal kinase) inhibitory peptide, Biochem. J. 434 (2011) 399–413.
[34] P. Philibert, A. Stoessel, W. Wang, A.P. Sibler, N. Bec, C. Larroque, et al., A focused antibody library for selecting scFvs expressed at high levels in the cytoplasm, BMC Biotechnol. 7 (2007) 81.
[35] D. Perez-Martinez, T. Tanaka, T.H. Rabbitts, Intracellular antibodies and cancer: new technologies offer therapeutic opportunities, Bioessays 32 (2010) 589–598.
[36] A. Kohl, H.K. Binz, P. Forrer, M.T. Stumpp, A. Plückthun, M.G. Grütter, Designed to be stable: crystal structure of a consensus ankyrin repeat protein, Proc. Natl. Acad. Sci. U. S. A. 100 (2003) 1700–1705.
[37] H.K. Binz, M.T. Stumpp, P. Forrer, P. Amstutz, A. Plückthun, Designing repeat proteins: well-expressed, soluble and stable proteins from combinatorial libraries of consensus ankyrin repeat proteins, J. Mol. Biol. 332 (2003) 489–503.
[38] H.K. Binz, P. Amstutz, A. Kohl, M.T. Stumpp, C. Briand, P. Forrer, et al., High-affinity binders selected from designed ankyrin repeat protein libraries, Nat. Biotechnol. 22 (2004) 575–582.
[39] A. Plückthun, Designed ankyrin repeat proteins (DARPins): binding proteins for research, diagnostics, and therapy, Annu. Rev. Pharmacol. Toxicol. 55 (2015) 489–511.
[40] D. Steiner, P. Forrer, M.T. Stumpp, A. Plückthun, Signal sequences directing cotranslational translocation expand the range of proteins amenable to phage display, Nat. Biotechnol. 24 (2006) 823–831.
[41] M. Schütz, A. Batyuk, C. Klenk, L. Kummer, S. de Picciotto, B. Gulbakan, et al., Generation of fluorogen-activating designed ankyrin repeat proteins (FADAs) as versatile sensor tools, J. Mol. Biol. 428 (2016) 1272–1289.
[42] P. Parizek, L. Kummer, P. Rube, A. Prinz, F.W. Herberg, A. Plückthun, Designed ankyrin repeat proteins (DARPins) as novel isoform-specific intracellular inhibitors of c-Jun N-terminal kinases, ACS Chem. Biol. 7 (2012) 1356–1366.
[43] A. Mann, N. Friedrich, A. Krarup, J. Weber, E. Stiegeler, B. Dreier, et al., Conformation-dependent recognition of HIV gp120 by designed ankyrin repeat proteins provides access to novel HIV entry inhibitors, J. Virol. 87 (2013) 5868–5881.
[44] A. Batyuk, Y. Wu, A. Honegger, M.M. Heberling, A. Plückthun, DARPin-based crystallization chaperones exploit molecular geometry as a screening dimension in protein crystallography, J. Mol. Biol. 428 (2016) 1574–1588.
[45] Y. Wu, A. Batyuk, A. Honegger, F. Brandl, P. Mittl, A. Plückthun, Rigidly connected multispecific artificial binders with adjustable geometries, Sci. Rep. 7 (2017) 11217.
[46] Y.S. Heo, S.K. Kim, C.I. Seo, Y.K. Kim, B.J. Sung, H.S. Lee, et al., Structural basis for the selective inhibition of JNK1 by the scaffolding protein JIP1 and SP600125, EMBO J. 23 (2004) 2185–2195.
[47] J. Liddle, P. Bamborough, M.D. Barker, S. Campos, C.W. Chung, R.P. Cousins, et al., 4-Phenyl-7-azaindoles as potent, selective and bioavailable IKK2 inhibitors demonstrating good in vivo efficacy, Bioorg. Med. Chem. Lett. 22 (2012) 5222–5226.
[48] S.K. Hanks, T. Hunter, Protein kinases 6. The eukaryotic protein kinase superfamily: kinase (catalytic) domain structure and classification, FASEB J. 9 (1995) 576–596.
[49] X. Liu, C.S. Zhang, C. Lu, S.C. Lin, J.W. Wu, Z.X. Wang, A conserved motif in JNK/p38-specific MAPK phosphatases as a determinant for JNK1 recognition and inactivation, Nat. Commun. 7 (2016) 10879.
[50] J. Chen, N. Sawyer, L. Regan, Protein–protein interactions: general trends in the relationship between binding affinity and interfacial buried surface area, Protein Sci. 22 (2013) 510–515.
[51] C. Greenman, P. Stephens, R. Smith, G.L. Dalgliesh, C. Hunter, G. Bignell, et al., Patterns of somatic mutation in human cancer genomes, Nature 446 (2007) 153–158.
[52] W. Kabsch, XDS, Acta Crystallogr. D Biol. Crystallogr. 66 (2010) 125–132.